Hindawi
International Journal of Energy Research
Volume 2023, Article ID 8825501, 15 pages
https://doi.org/10.1155/2023/8825501

Research Article

Conceptual Design of a Novel Megawatt Molten Salt Reactor Cooled by He-Xe Gas

Hongkai Zhao[1,2,3] **Jianhui Wu**[1,2,3] **Shuning Chen**[1,2,3] **Yong Cui**[1,2] **Jingen Chen**[1,2,3] **and Xiangzhou Cai**[1,2,3]

[1]*Shanghai Institute of Applied Physics, Chinese Academy of Sciences, Shanghai 201800, China*
[2]*CAS Innovative Academy in TMSR Energy System, Chinese Academy of Sciences, Shanghai 201800, China*
[3]*University of Chinese Academy of Sciences, Beijing 100049, China*

Correspondence should be addressed to Jingen Chen; chenjg@sinap.ac.cn and Xiangzhou Cai; caixiangzhou@sinap.ac.cn

Received 21 June 2023; Revised 4 September 2023; Accepted 8 September 2023; Published 12 October 2023

Academic Editor: Samuel Lalthazuala Rokhum

He-Xe gas-cooled micro-molten salt reactor (HX-micro-MSR) is a novel reactor concept that integrates the technologies of molten salt reactor and closed Brayton cycle (CBC), which has a more compact structure compared with the other types of micro-MSRs. The reactor system probed in this paper has a thermal power of 2.5 MWth and consists of the core, fission gas collecting container, and CBC system. The He-Xe gas flows through the coolant channels in the core to transfer the nuclear heat to the CBC for electricity production. To withstand the large pressure difference between the He-Xe gas coolant (7 MPa) and molten salt (nearly atmospheric pressure), the sizes and wall thickness of coolant channels are analyzed and optimized to be 8 mm and 0.5 mm, respectively. In total, 1050 coolant channels are regularly arranged in the core to effectively remove the nuclear heat. The enrichment of U-235 in the fuel UF_4 is determined to be 61% to meet the burnup goal of 5 years. To minimize the neutron leakage, the thickness of reflector is selected to be 23 cm. Six control drums with the diameter in 10.5 cm and neutron absorber layer thickness in 1 cm are symmetrically placed in the reflector to realize reactivity control under both normal and accident conditions. Radiation shield is designed and analyzed by varying the thickness of multiple shielding layers, and it is found that a combination of W layer in 14 cm and $Mg(BH_4)_2$ layer in 56 cm can satisfy the criterion of radiation dose (<1 mSv/h). The total weight of HX-micro-MSR is estimated to be 35 tonnes and falls into the acceptable range.

1. Introduction

Molten salt reactor (MSR) is one of the six candidates of Generation IV nuclear reactor systems [1] and possesses unique advantages in the aspects of safety, economy, non-proliferation, and fuel utilization, thanks to the application of molten salt. Up until now, a series of concepts of molten salt reactor has been proposed, which can be generally divided into two sorts according to the types of fuel: solid-fueled MSRs and liquid-fueled MSRs. Liquid-fueled MSRs adopt the molten salt dissolved with the fissile and fertile elements as both the fuel and coolant. Compared with the solid-fueled MSRs, i.e., FHR (fluoride salt-cooled high-temperature reactor) [2] in which molten salt acts as coolant for solid fuel pebbles or fuel rods [3–6], liquid-fueled MSRs are exempt from manufacture of fuel elements and thereby have advantages in simplification and miniaturization of core structure. Solid-fueled MSRs might be accidentally compacted because of bumps in transit, which would lead to local criticality risk caused by the local increase in fuel density, but this is not an issue for the liquid-fueled MSRs. Meanwhile, liquid-fueled MSRs are capable to perform online refueling and reprocessing [7]. Compared with the online refueling of CANDU (Canada Deuterium Uranium) and AGRs (advanced cooling reactors) by replacing the prepared fuel elements, liquid-fueled MSRs would be more flexible to control reactivity by adjusting the concentration and proportion of nuclide in the fuel salt. A great initial reactivity to compensate for reactivity loss due to burnup during operation in solid-fueled reactors is unnecessary in liquid MSRs, because MSRs can maintain core criticality by online adding the fuel. The possibly leaked molten salt arising from the

accidents of support structure break can quickly solidify due to its high melting point. A high inherent safety is hence usually associated with the liquid-fueled MSRs and attracts growing attention in the field of micronuclear reactors, which usually have an output power lower than 20 MWe [8] and can operate as a microgrid to produce electricity [9, 10].

Microminiaturization of liquid-fueled MSRs can be dated back to the program of aircraft nuclear propulsion (ANP) launched by the USA in the 1950s. A 2.5 MWth MSR, termed as aircraft reactor experiment (ARE), was built and successfully operated for around 100 h with the aim to test the feasibility of fluid-fuel, high-temperature, high-power density reactors for the propulsion of supersonic aircraft [11, 12]. With the increasing demand for the exploration of ocean/space and off-grid electricity supply for remote areas, micro-MSR has recently become a hot spot of MSR study. Various conceptual designs of micro-MSRs have been put forward worldwide, and most of them belong to the heat pipe- (HP-) cooled reactors [13, 14]. An HP is a sealed pipe with the working fluid continuously circulating inside in a nature way to transfer the heat from the hot-end to cold-end. The structure of HP is simple while having a good performance in heat transfer. However, the scale of power taken away by a single HP is severely limited by various parameters including capillary forces, choked flow, interfacial shear, and incipient boiling. As a result, hundreds of HPs usually have to be installed in the core for a micro-MSR with the core power up to 1 MWe, which would significantly complicate the core structure since dedicated heat exchangers matching HPs are required to be installed above the core to transfer the heat from the HPs to thermoelectric conversion system. On account of these factors, most of the HP-cooled micro-MSRs reported in the open literature are in kilowatt scale. Thereby, it is necessary to explore new cooling mode for the core of megawatt micro-MSRs, which are expected to be applied for electricity supply in multiple scenarios.

A closed Brayton cycle (CBC) system is an integrated thermoelectric conversion system with all components connected by the gas coolant in a closed loop. An intermediate heat exchange loop instead of HPs is applied in the core. Most importantly, it is free to punch large number of holes on the core vessel since the gas coolant can be collected at the upper plenum of core and guided outside the core through one channel. Employing CBC would be an effective way to address the issues that arise in the HP-cooled micro-MSRs. A typical CBC and its temperature entropy diagram are shown in Figure 1 [15]. The gas working fluid heated by the reactor core enters turbine driving dynamo, where the heat contained in the gas working fluid is converted to mechanical energy from (1) to (2). Afterwards, the gas is disposed by the other parts to the state (6) for next cycle. CBC can work in a wide power range from megawatts to gigawatts with the thermoelectric conversion efficiency higher than 40% [16], which fully covers the power scale of micro-MSRs.

Helium gas is one of inert gases possessing excellent thermal properties in the aspect of thermal conductivity, dynamic viscosity, and so on. It is the preferred working fluid for the CBC and is widely adopted by the terrestrial nuclear power plants, such as high-temperature gas-cooled reactor and gas-cooled faster reactors [17, 18]. However, the molecular weight of helium is quite low, and a great number of turbomachine stages are required to compress it to a value meeting the requirement, leading to a large size and heavy weight of turbomachine. Xenon (Xe) has an atomic weight of 131, and it is mixed with helium in a ratio ranging from 15 g/mol to 40 g/mol, significantly reducing the number of turbomachine stages while maintaining the main thermal properties of helium [19, 20]. The He-Xe binary mixture has been widely used in the design of micro-solid-fueled reactors [21, 22]. High-pressure helium might diffuse through the metal and subsequently lead to metal embrittlement. This phenomenon can be avoided by improving the manufacturing techniques, such as coating the metal with a thin film of particular material [23].

In this study, a 2.5 MWth He-Xe gas-cooled micro-MSR (HX-micro-MSR) is designed and optimized under the criteria/requirements of micronuclear reactors as listed in the following:

(1) The size of reactor system should be smaller than $2.432 \times 2.532 \times 6\,m^3$ to be loaded by the standard container of trucks for transport

(2) The weight of reactor system should be lower than 38 tonnes to comply with the constraints of land transportation [24]

(3) The fuel lifetime is around 5 years to enhance the economy and reduce the risk of radiation leakage during refueling process

(4) The core shutdown margin should be greater than or equal to \$7.85 [25]

(5) The fuel temperature coefficient should be negative to ensure the safety of reactor system

(6) The radioactivity equivalent dose should be lower than 1 mSv/h (0.1 rem/h) to protect staff in the working area

2. Reactor System and Core Configuration

2.1. System Overview. The thermal power of HX-micro-MSR is designed to be 2.5 MWth. With the thermal efficiency of 40% due to the outlet temperature higher than 1100 K, the electrical power is 1 MWe, which is a typical power scale of microreactor. The reactor system consists of three main functional components, i.e., fission gas extraction module, reactor core, and energy conversion module in CBC as shown in Figure 2. Fission gas extraction module functions to collect the sparingly soluble fission gases, including xenon and krypton, and inject them into the shielding layer to act as a neutron absorption material. In this way, parasitic neutron absorption resulting from fission gases can be significantly reduced. Meanwhile, the heat of shielding layer resulting from neutron and gamma rays irradiation can be

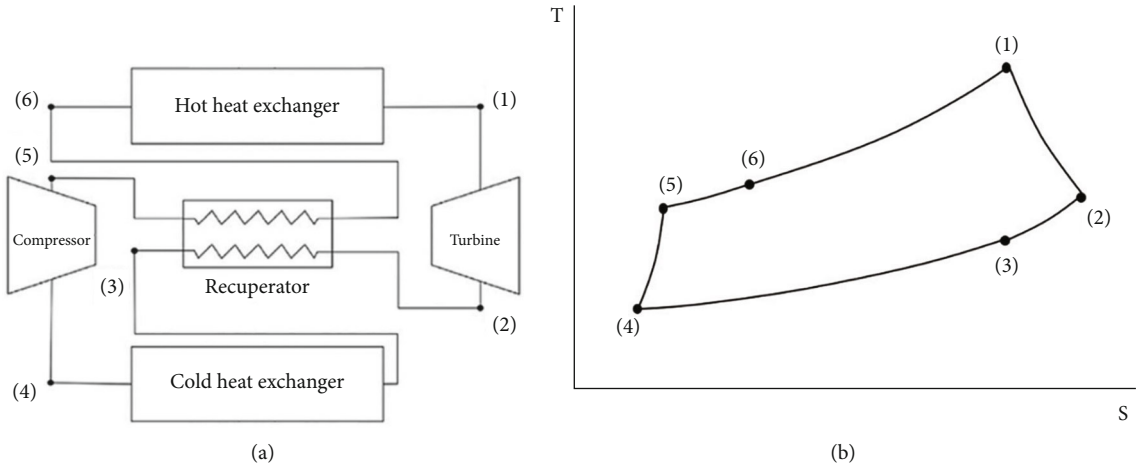

Figure 1: Typical CBC (a) and temperature entropy diagram (b).

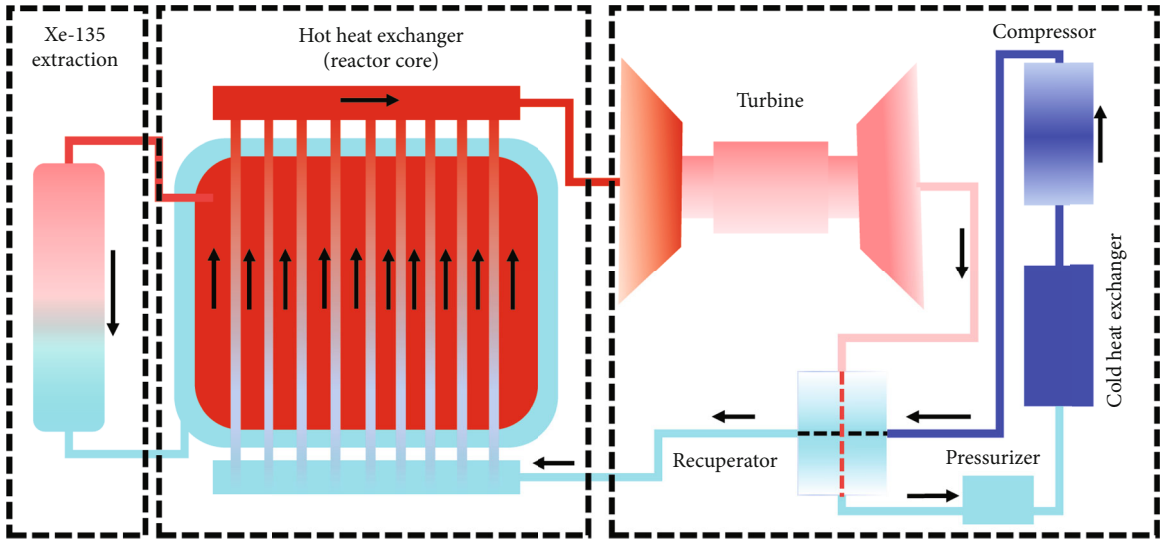

Figure 2: The overview of the HX-micro-MSR.

removed by the pressurized fission gases with a low temperature [26]. Regarding leakage of helium, its compensation can be achieved by the gas pressurizers and reservoirs. During the operation, He-Xe gas coolant circulates through the core, and the fission energy is continuously converted into electricity by the energy conversion module.

2.2. Reactor Core Configuration. The configuration of reactor core is shown in Figure 3. From inside to outside, the reactor core is divided into active core zone, reflector zone, and shielding zone. The active core zone consists of He-Xe coolant conduits and their surrounding molten fuel salt, functioning to produce and export the nuclear energy for electricity generation. The reflector zone is made of BeO with six control drums regularly arranged in it to reduce neutron leakage and control core reactivity. The shielding zone is placed outside the reflector zone to protect staff and electronic equipment from radiation damage.

The main parameters of core are listed in Table 1. The specific geometrical parameters which determine the neutronic performance of core will be optimized in the following sections and summarized at the end of paper. The same fluoride molten salt dissolved with fuel elements (71.7% LiF–16% BeF_2–12.3% UF_4, mol%) is adopted to inherit the main merits of traditional MSRs. The melting and boiling point of this fuel salt are around 723 K and 1673 K, respectively, which provide a wide range of temperature option for core operation [7, 27]. However, it is well known that raising the core operational temperature would enhance the thermal efficiency but meanwhile aggravate corrosion and neutron irradiation damage of structure materials. By balancing these two effects, 1200 K is chosen as the core operational temperature with referring to the core design of gas-cooled reactors [28]. The inlet temperature of He-Xe gas is set to be 823 K, around 50 K higher than the melting point of fuel salt to prevent the fuel salt from

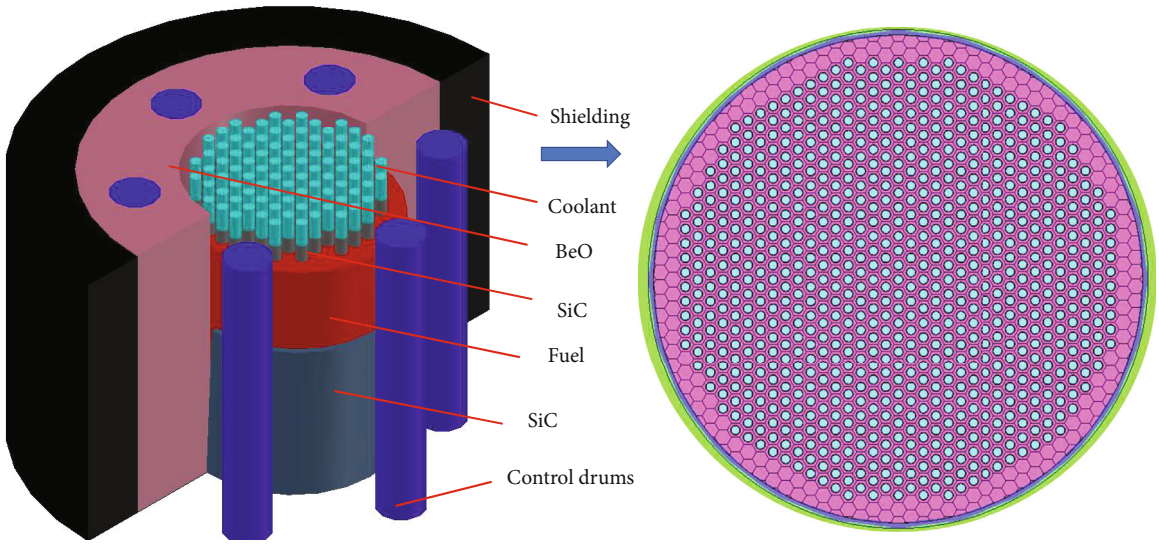

Figure 3: Specific core structure of the HX-micro-MSR.

solidification during core operation. The He-Xe mass flow rate is determined by the thermal efficiency of CBC system which, on the other hand, is influenced by the core outlet temperature and existing CBC technologies. By extensively reviewing the designs of He-Xe-cooled reactors, it is found that the He-Xe mass flow rate of most reactors falls into the range of 7 to 50 kg/sec [28]. In this study, an outlet core temperature of 1123 K is chosen, slightly lower than the core operating temperature to enhance the thermal efficiency.

Total 60 L FLiBe fuel salt is contained in the core and is kept constant as optimizing the core size in the following sections to keep the thermal power density unchanged. Because of the fast neutron spectrum and small core size, the enriched uranium with the U-235 content higher than 20% is applied to maintain the core critical operation. The abundance of Li-7 in Li of FLiBe fuel salt is 99.995% by balancing the parasitic neutron absorption and Li purification cost, and the neutron absorption of tritium generated from such Li-6 concentration also has slight effect on the reactivity of the core [29].

Silicon carbide is characterized by its high heat resistance, high irradiation resistance, low neutron absorption, etc. [30] and is considered as one of the most promising cladding materials applied in the reactor core. There are several industrial fabrication and welding processes available, such as high-temperature sintering [31], which are expected to address the issues of SiC tube manufacture. In this design, it is adopted as the cladding of coolant channel to withstand corrosion at a high pressure and high temperature [32]. The He-Xe gaseous coolant wrapped by the SiC pipe is composed by 72 mol% He and 28 mol% Xe with a molar mass of 40 g/mol, which has best thermal properties in mixture of He and Xe, such as thermal conductivity and dynamic viscosity [33]. To achieve a high thermal efficiency, the working pressure of the coolant is set to be 7 MPa, at which its density is 0.0365 g/cm^3. However, under such a high pressure, additional measures are required to ensure hermeticity against the gas diffusion including coating and metal lining inside the tube [31], which will be studied in our future work.

BeO has a large neutron scattering cross section, a small neutron absorption cross section, and, most importantly, a high melting point (1400 K). It is adopted as the reflector of HX-micro-MSR. B_4C with the B-10 enrichment of 90% is taken as the neutron absorber of control drums. A preliminary shielding design is proposed in this work; from inner to outer, fission gas layer, multiple radiation shielding layer and stainless-steel layer are designed to effectively shield the neutron and gamma. Since the fission gas Xe-135 extracted from the core has a large neutron absorption cross section [34], the fission gas layer is expected to save the shielding material and consequently decrease the weight and size of the core. With considering Xe-135 generated in the core while decayed and neutron-absorbing in the fission gas layer, the equilibrium concentration of Xe-135 can be calculated as follows:

$$N_{\mathrm{Xe}}(\infty) = \frac{\gamma \Sigma_{\mathrm{f}} \phi_{\mathrm{c}}}{\lambda_{\mathrm{Xe}} + \sigma_{\mathrm{a}}^{\mathrm{Xe}} \phi_{\mathrm{o}}}, \tag{1}$$

where γ is the fission yield of Xe-135 and I-135, Σ_{f} is the macroscopic fission cross section, ϕ_{c} is the neutron flux in core, λ_{Xe} is the decay constant of Xe, $\sigma_{\mathrm{a}}{}^{\mathrm{Xe}}$ is the macroscopic absorption cross section, and ϕ_{o} is the neutron flux in fission gas layer.

3. Calculation Tools and Methods

In this study, two software, Ansys [35] Workbench 18.0 and SCALE 6.1 [36], are used for thermal hydraulics and neutronic calculation, respectively. Ansys Workbench is a specialized finite element analysis platform developed by Ansys Company in the United States. It integrates various application programming interfaces (API) that have different functions. Users can freely combine them and realize

Table 1: Main parameters of the HX-micro-MSR core.

Parameters	Specification
Thermal/electrical power (MW)	2.5/1
Fuel	LiF-BeF_2-UF_4
Composition (mol%)	71.7%-16%-12.3%
Density at 1200 K (g/cm^3)	3.10
Expansion coefficient (g/cc/K)	$6.70E-4$
Li-7 concentration (%)	99.995
Melting point (K)	773
Volume (L)	60
Mass (tonne)	0.189
Coolant pipes (SiC)	
Elasticity modulus (GPa)	420
Poisson ratio	0.14
Strength of extension (MPa)	214~450
Coefficient of thermal expansion (g/cc/K)	$4.90E-06$
Specific heat at constant pressure (J/(kg·K))	1920
Thermal conductivity (W/(m·K))	123
Coolant (He-Xe)	
Molecular weight of mixture (g/mol)	40
Pressure (MPa)	7
Kinetic viscosity (μPa/s)	32.857 (400 K)–74.286 (1200 K)
Specific heat at constant pressure (J/(kg·K))	535.70 (400 K)–519.70 (1200 K)
Thermal conductivity (W/(m·K))	0.08409 (400 K)-0.18340 (1200 K)
Reflector (BeO)	
Density (g/cm^3)	2.84
Melting point (K)	2803-2843
Control drums (B_4C)	
Density of B_4C (g/cm^3)	2.52
Number of drums	6
Shielding layer	
Density of Hastelloy (g/cm^3)	8.29
Concentration of Xe-135 (atom/cm^3)	$4.80E+15$
Density of tungsten (g/cm^3)	18.50
Density of $Mg(BH_4)_2$ (g/cm^3)	1.48
Density of SS316 (g/cm^3)	8.03

seamless data transmission, providing a high degree of freedom and scalability. The components Static Structural and Fluent are adopted in this study to optimize the size and number of SiC pipes to withstand the pressure and meet the heat transfer requirements as well.

SCALE 6.1 is a code program developed by Oak Ridge National Laboratory (ORNL) for critical safety and reactor physics analysis. It contains several computational modules, including CSAS6, SMORES, ORIGEN-S, and MAVRIC, which function for calculations of different neutronic aspects. In this study, CSAS6 and MAVRIC are used for core critical analysis and shielding calculation, respectively. Critical calculation of CSAS6 will provide a source of radioactivity to MAVRIC module for shielding calculation. Nuclear data library ENDF/B-VII.0 is chosen for neutronic calculations.

Core burnup calculation is carried out by using an in-house fuel burnup calculation code, MODEC (Molten salt reactor specific high-fidelity depletion Code), which was developed specially for MSRs and is capable of simulating the processes of online refueling and reprocessing [37]. The code system of MODEC solves the burnup equations involved in MSRs using two advanced depletion algorithms: the transmutation trajectory analysis (TTA) and the Chebyshev rational approximation method (CRAM), having a high fidelity and precision. Up to now, it has been extensively applied for fuel burnup calculation of different types of MSRs [38–40].

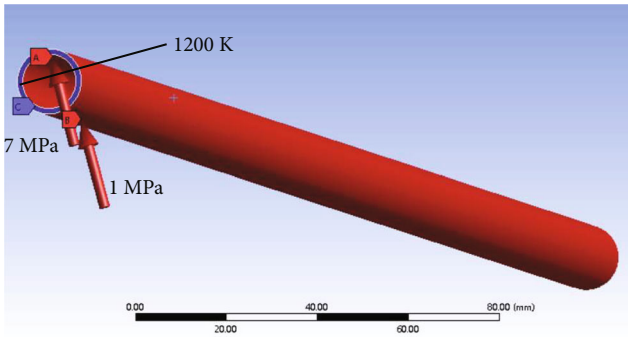

Figure 4: The stress load of pipe.

4. Results and Discussion

As a new concept of reactor, extensive analysis on the core geometrical parameters is necessary to ensure that the designed core satisfies the criteria. In this section, the main geometrical parameters of HX-MSR core, including SiC pipes, reflector, control drums, and shielding layer, are successively analyzed in terms of the core neutronic performance. The enrichment of U-235 in the uranium fuel salt is also studied to achieve the burnup goal of 5 years.

4.1. SiC Pipes

4.1.1. Mechanical Analysis. As mentioned above, SiC pipes in the core have to bear a pressure of 7 MPa under the operational temperature of 1200 K during core operation. To ensure the structural integrity and safety of SiC pipes, mechanical analysis is conducted by varying the wall thickness and diameter of pipes. A material reliability measure factor, FOS (factor of safety), is taken for safety evaluation of pipes. FOS is defined as the ratio of the ultimate stress a_u to the working stress a_w of the component material (FOS = a_u/a_w), which should be greater than 1. To ensure the integrity of any point along the pipe, maximum Mises stress in the axial direction of the pipe is taken as the working stress. Here, Mises stress can be calculated by

$$a_{\text{Mises}} = \sqrt{\frac{(a_1 - a_2)^2 + (a_2 - a_3)^2 + (a_3 - a_1)^2}{2}}, \quad (2)$$

where a_1, a_2, and a_3 indicate the first, second, and third principal stresses, respectively. Ultimate stress refers to the maximum stress withstood by the material and can be calculated by using Ansys based on the tensile yield strength and compressive yield strength, which are 382 MPa and 2000 MPa for SiC, respectively [41, 42].

Figure 4 demonstrates a schematic diagram of pipe loaded with the pressure and temperature. A 7 MPa uniform pressure is loaded on the inner wall of the pipe (A), while the outer wall of the pipe is under ambient pressure (B). To simplify the calculation model, all the pipes in the core are assumed to be the same and free to deform, and the gravity is neglected in calculation. Since SiC pipes in the HX-microreactor core would be hold by the support plates, the bending strength is small and imposes neglectable influence

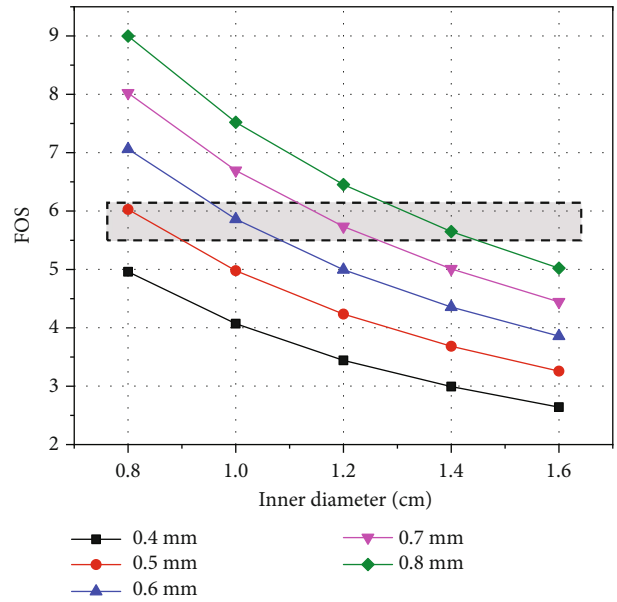

Figure 5: FOS of different inner diameter and thicknesses.

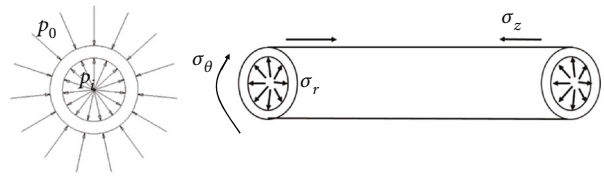

Figure 6: Schematic diagram of pipeline cross section.

on FOS, indicating the independence of FOS with the pipe length. The SiC pipe length in 50 cm of an initial core before optimization is hence taken for calculation. The SiC thermal expansion coefficient of $4.9E-06$ g/cc/K under 1200 K is taken for calculation. The axial minimal FOS varying with the wall thickness and inner diameter of the pipe is shown in Figure 5. The FOS of SiC pipes increases with its thickness while declines with its inner diameter, which consists with the law of elastic mechanics and can be deduced from the stress equations as follows:

$$\sigma_\theta = \frac{P_i R_i^2 - P_0 R_0^2}{R_0^2 - R_i^2} + \frac{(P_i - P_0) R_i^2 R_0^2}{R_0^2 - R_i^2} \frac{1}{r^2}, \quad (3)$$

$$\sigma_r = \frac{P_i R_i^2 - P_0 R_0^2}{R_0^2 - R_i^2} - \frac{(P_i - P_0) R_i^2 R_0^2}{R_0^2 - R_i^2} \frac{1}{r^2}, \quad (4)$$

$$\sigma_z = \frac{P_i R_i^2 - P_0 R_0^2}{R_0^2 - R_i^2}, \quad (5)$$

where P_i and P_0 are the pressures exerted on the inner and outer wall of pipes, respectively, as shown in Figure 6; R_i and R_0 represent the inner and outer diameter of pipes, respectively; r is the distance between two point on the central axis of pipes; and σ_θ, σ_r, and σ_z are the stresses in three different directions at point r in the cylindrical coordinate system (as shown in Figure 6).

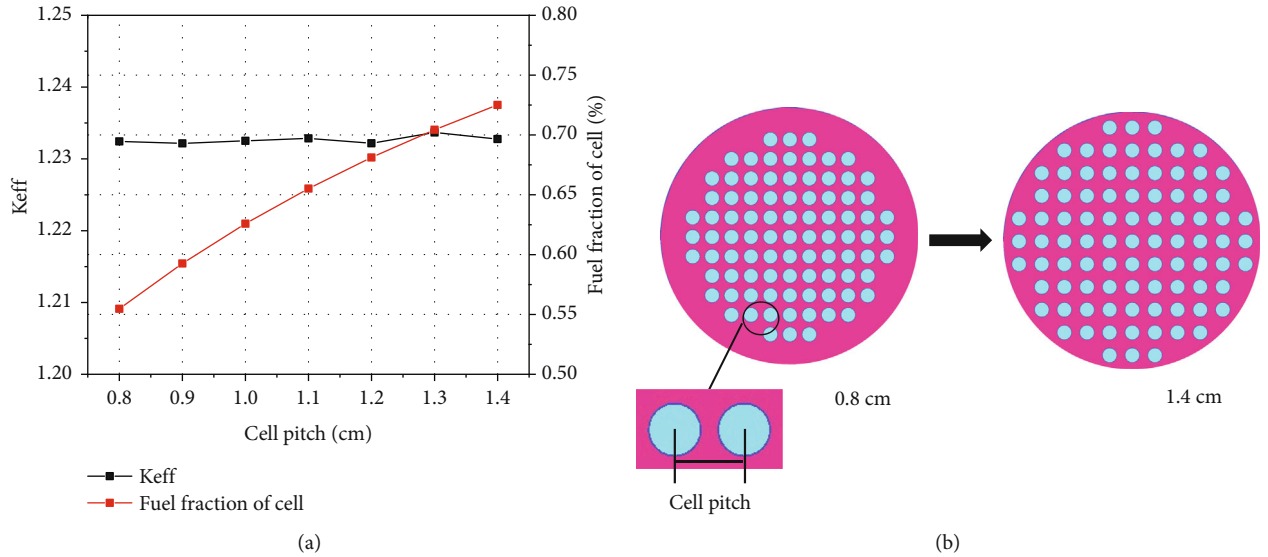

Figure 7: Effect of cell pitch on k_{eff} (a) and schematic diagram of pipe spacing variation (b).

In general, the requirement for FOS in a given field is a complex process, involving various factors such as the service condition, type of materials, and industrial standard. To conservatively ensure the integrity of the SiC pipes and meanwhile balance the capability of heat transfer, FOS around 6 is selected [43], which is highest of the pressure vessels (FOS in 4-6). The optional region that satisfies the criteria is highlighted in Figure 5 by shadow for further geometrical analysis.

4.1.2. Pipe Arrangement in the Core. Cell pitch is an important parameter that potentially impacts the neutronic performance of the core [44, 45]. Its influence on k_{eff} is investigated by changing the pipe pitch from 0.8 cm to 1.4 cm with the pipe diameter remaining 1.6 cm. It should be noted that the core size and total fuel volume is fixed during calculation, and the enrichment of U-235 in uranium is 42%. As demonstrated in Figure 7, k_{eff} slightly changes with the pipe pitch, indicating quite limited influence of pipe pitch on the neutronic performance, mainly due to the harden neutron spectrum of the core and negligible impact of SiC on neutron moderating. Although pipe pitch in the core might influence the local temperature distribution and in turn the local power distribution, this effect will be mitigated for HX-micro-MSR due to natural convection of fuel salt driven by the temperature difference, from which it can be concluded that the influence of pipe pitch on core pipe arrangement is negligible.

Subsequently, core pipe arrangement with varying the number, thickness, and diameter of pipes is extensively analyzed by using the Ansys Fluent. Three arrangements are finally screened out (as summarized in Table 2) to meet the requirements of total mass flow, inlet temperature, outlet temperature, and FOS. The cases in which the pipe inner diameter is larger than 1.2 cm, as depicted in Figure 7, are not selected since the number of pipes that can be arranged in the core is limited and cannot meet the objective of thermal hydraulics.

Table 2: Main parameters of the SiC pipes.

Groups	Core-1	Core-2	Core-3
Inner radius (cm)	0.4	0.5	0.6
Thickness (mm)	0.5	0.6	0.7
Length (cm)	24.5	23.3	22.4
Safety factor	6.1	5.7	5.7
Number of pipes	1050	667	424
Radius of core (cm)	24.5	23.3	22.4

To evaluate the safety of HX-micro-MSR, the temperature reactivity coefficients are preliminarily analyzed for the above three cores by raising the core operational temperature from 1000 K to 1400 K. Deep negative temperature reactivities of -5.72 pcm/k, -5.63 pcm/k, and -5.50 pcm/k are obtained for Core-1, Core-2, and Core-3, respectively, due to large fuel expanding effect and Doppler effect as increasing the temperature. Small difference among them can be attributed to the different neutron leakage resulting from the different core sizes.

4.2. Reflector Analysis. The core reflector functions to reflect part of neutrons back to the core and in turn reduce the neutron leakage to improve neutron economy. This property increases with core reflector thickness, which however would lead to an increment of the core mass. Figure 8 shows the neutron leakage rate and total mass of three cores changing with the thickness of reflector. The neutron leakage rate decreases dramatically as raising the reflector thickness up to around 23 cm, indicating more efficiency of unit length of reflector in this range. After 23 cm, the effect of reflector tends to be saturated, and the decline in leakage is slowing down gradually. Relatively low neutron leakage for Core-1 can be attributed to its smaller ratio of surface area to volume. Combined with the factor of leakage rate and temperature reactivity coefficient, Core-1 is hence selected for the

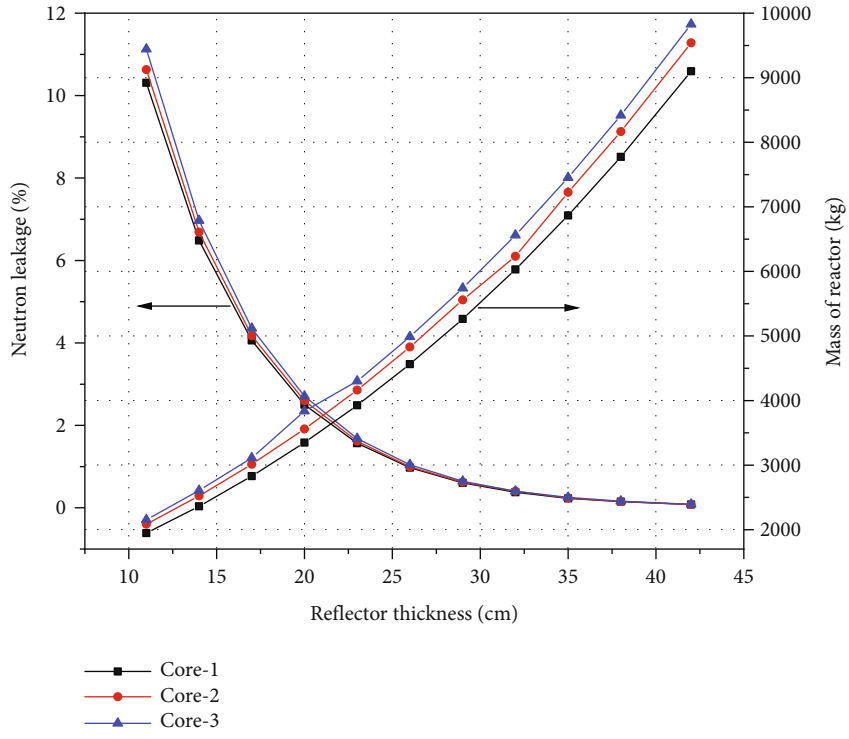

Figure 8: Effect of reflector thickness on leakage rate and total reactor mass.

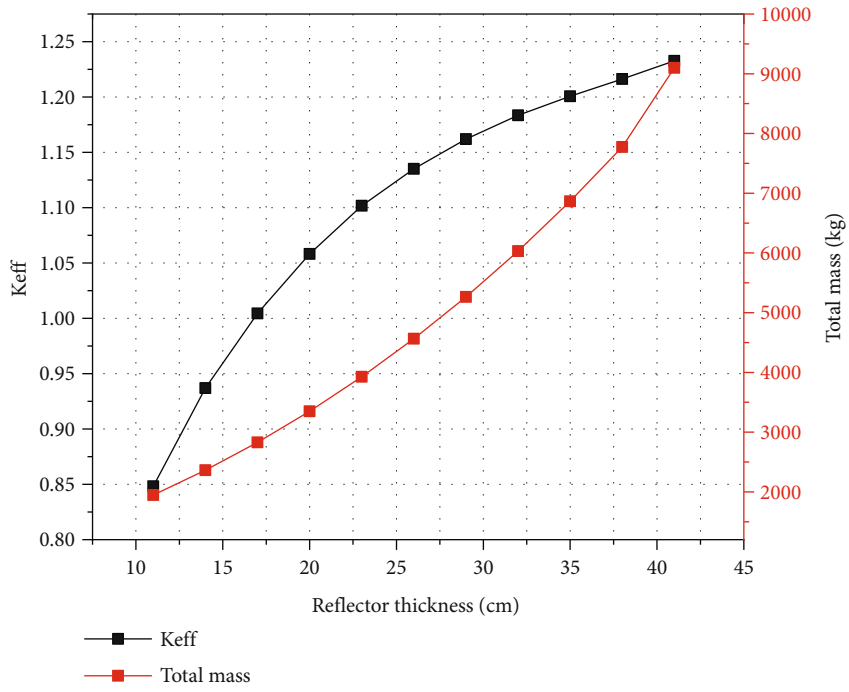

Figure 9: Variation of k_{eff} and core total mass with reflector thickness.

design of HX-micro-MSR, and its k_{eff} and neutron leakage rate changing with the reflector thickness are demonstrated in Figure 9. By balancing the neutron leakage rate, initial excess reactivity, and core mass, 23 cm is selected for the reflector thickness.

4.3. Burnup Analysis and Control Drum Design. The enriched uranium with the U-235 content lower than 20% would be insufficient to maintain the core critical operation because of the fast neutron spectrum and small core size which would lead to a large neutron leakage. Therefore, to

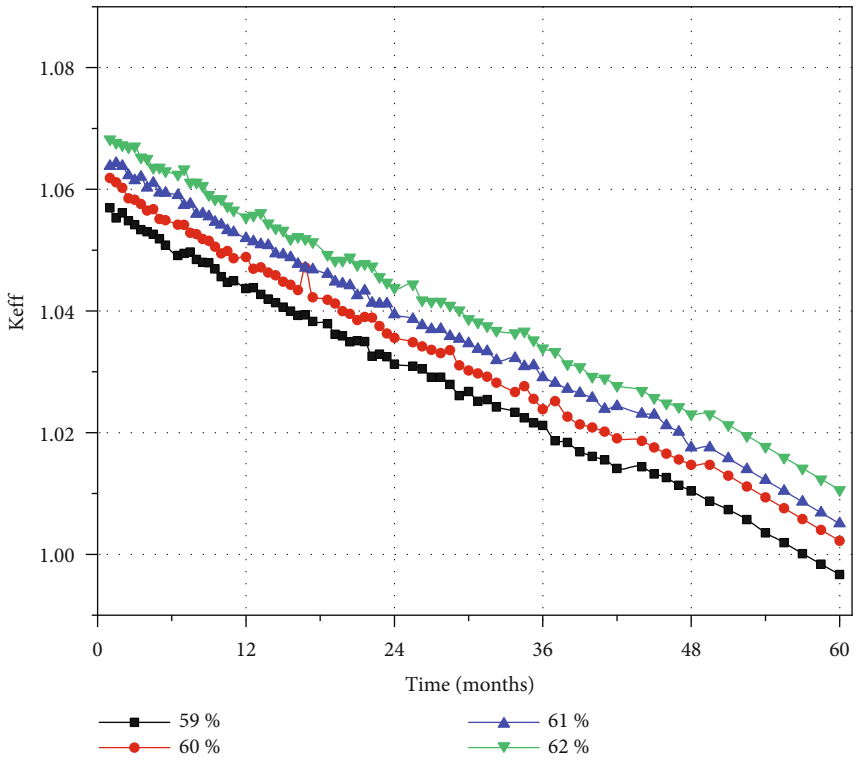

Figure 10: Variation of k_{eff} with burnup.

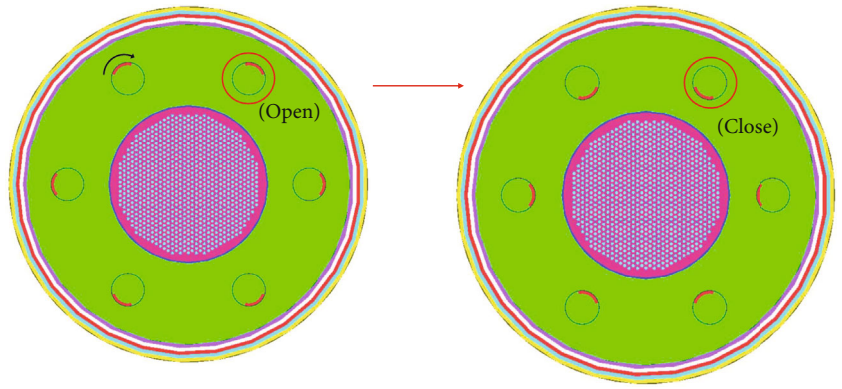

Figure 11: Layout of the control system.

achieve the burnup goal of 5 years, U-235 enrichment in uranium varying from 59% to 62% is investigated for Core-1. It should be noted that using such a high-enriched uranium fuel (HEU) would cause the problem of nuclear proliferation, which is the research topic in our future to apply other alternative fuels, such as Th-U fuel, to enhance the nonproliferation. As demonstrated in Figure 10, around 6000 pcm decreases after 5 years of operation with a power of 2.5 MWth. Considering the reactivity reduction introduced by the control drums, U-235 enrichment of 61% with a reactivity of 200 pcm left at the end of cycle (EOC) is selected by balancing the reactivity control.

The control system in the reactor functions to regulate the power and shut down the core during accidents. It is composed by the control drums for HX-micro-MSR. Layout of the control drums is shown in Figure 11. Sufficient reactivity reduction should be introduced by the control drums to ensure the safety of the reactor under accidents, especially for the accidents that the reactor falls into a lake or ocean. In these accidents, the reactor will be submerged in the water or wet stand and the neutron spectrum in the reactor subsequently is thermalized, leading to a significant increase of reactivity [46]. To handle this safety issue, a core shutdown criterion with k_{eff} less than 0.95 has been proposed for a lithium heat pipe-cooled reactor according to the safety analysis of an accident of submersion [25]. This criterion has been adopted by many follow-up studies [25, 47, 48], and it is hence taken for the safety design of the HX-micro-MSR.

As demonstrated in Figure 11, six control drums are adopted and located at each vertex of the regular hexagon. The center of control drums is 18.25 cm away from the center of core. The neutron absorption layer B_4C of control

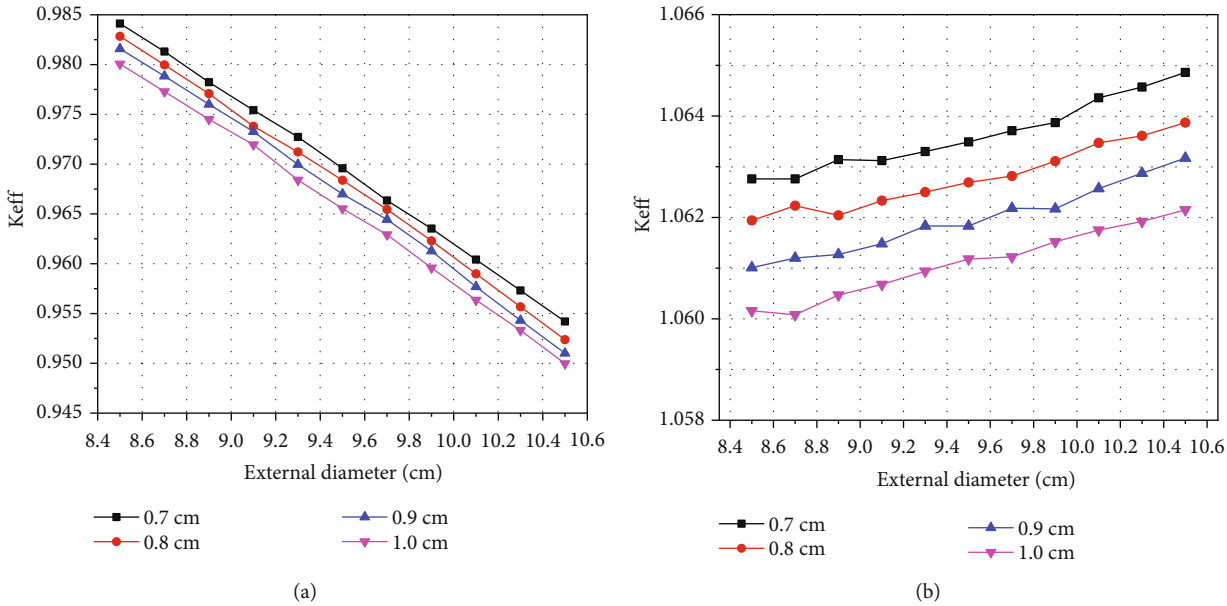

FIGURE 12: Variation of k_{eff} with outer diameter and absorption layer thickness of control drum as opening (b) and closing (a) the control drum.

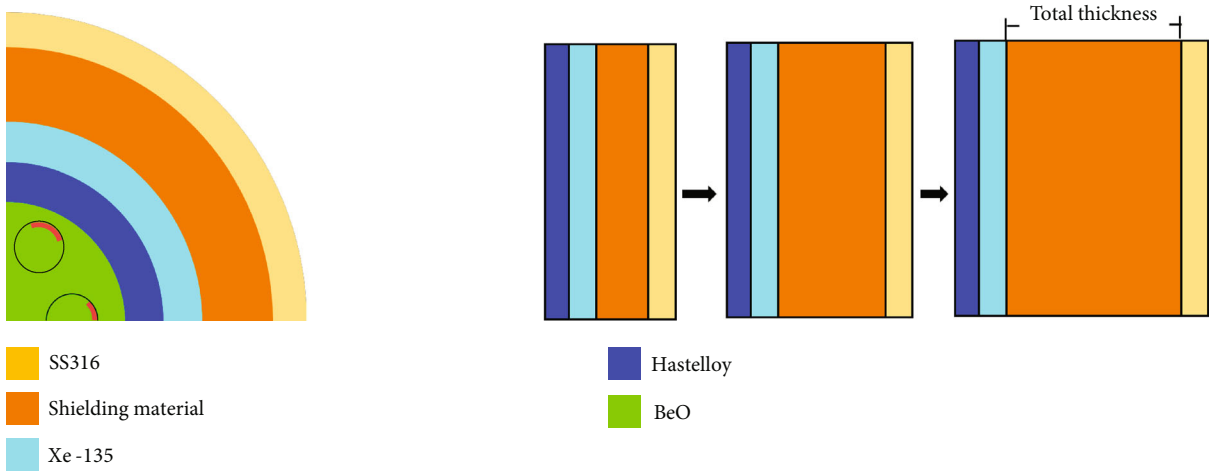

FIGURE 13: Shielding layer setting and schematic diagram of thickness change of shielding layer.

drum is in a quarter ring with a certain thickness as labeled in red in the control drum. The motion of control drum is driven by a spring device in the center of control drum, and the B_4C layer can turn inward automatically without external force (close state). Since the size and B_4C layer thickness of the control drum would significantly affect the core reactivity, they are investigated in terms of k_{eff} as shown in Figure 12. Greater influence on the core reactivity would be introduced as increasing the diameter of control drum, since the absorption layer of control drum will be closer to (farther from) the active core at closing (opening) state of the control drums. This effect would be enhanced by increasing the thickness of absorption layer. Considering the neutronic economy and reactivity stability caused by maneuvering the control drums, 1.0 cm in thickness of absorption layer and 10.5 cm in diameter of control drum are adopted to meet the design criterion 4.

4.4. Radiation Shielding Design. Radiation shielding of reactor functions to protect the humans and devices from neutron and photon (e.g., gamma ray) irradiation damage. It is particularly important for the microreactors due to their large neutron leakage and potential applications in populated areas. Radiation shielding design of microreactors should satisfy the criteria of radiation dose and limitation of core size and weight [49]. According to the study of Li [50], the maximum radiation dose exposed to professionals should be no higher than 1 mSv/h (0.1 rem/h).

The specific layout of material layer surrounding the active core is shown in Figure 13. The layer closest to the reflective layer is Hastelloy, which is a high-temperature, radiation-resistant, high-strength nickel-based alloy and here acts as the support material for the first layer. The second layer is composed of Xe-135 gas, which is a fission gas extracted from the core with the concentration of 4.8 ×

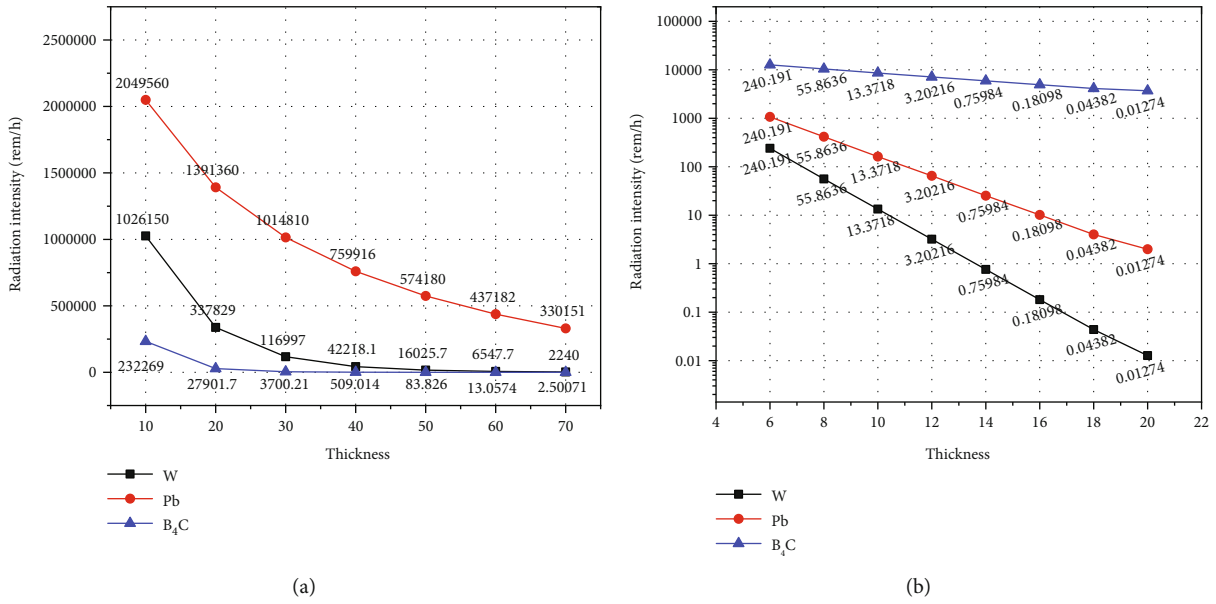

Figure 14: Comparison of W, Pb, and B_4C neutron (a) and photon (b) shielding performance.

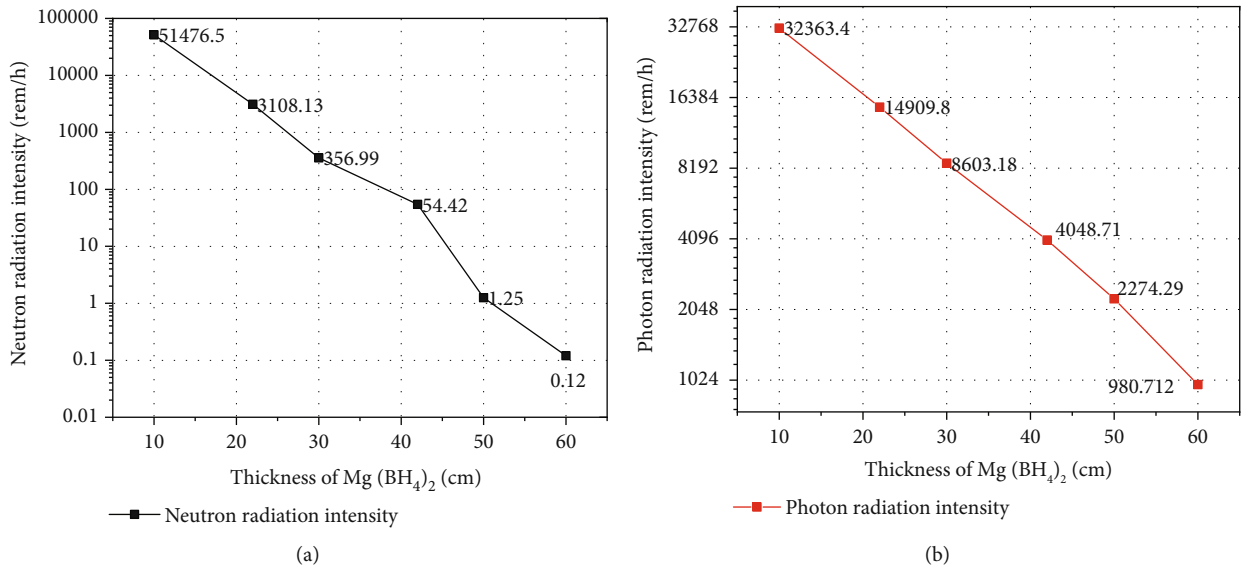

Figure 15: Neutron (a) and photon (b) shielding performance of $Mg(BH_4)_2$.

10^{15} atom/cm^3. Because of the large neutron absorption cross section of Xe-135, the neutron flux declines by 2.7×10^{10} cm^{-2}·s^{-1} (~2.6%) with a thickness of 0.5 cm absorption layer, which is remarkable on neutron shielding. The material layer specialized to shield neutron and photon is placed outside the fission gas layer. Stainless steel SS316 is employed as the structural material and formed the outermost layer.

In general, neutrons can be effectively shielded by the materials composed of light nuclei, while heavy nuclei materials are required to shield the photons. W, Pb, and B_4C are three commonly used shielding materials, and their shielding effects are individually investigated by separately setting them as the radiation shielding layer as demonstrated in Figure 14. The detectors for all cases are placed in the spots 100 cm away from the outer shield surface. Total 27 neutron groups and 19 photon groups are taken to calculate the response functions of ANSI standard. The mass of the reactor can be calculated according to the nuclide concentration in SCALE and the volume automatically obtained. As shown in Figure 14, a single material cannot meet both shielding requirements at one time. For instance, B_4C is more prone to shield the neutron while W has a strong ability to shield the photons. Compared with W and Pb, B_4C has a lowest density (2.51 g/cm^3), which would benefit for core weight limitation, but it is difficult to satisfy the shielding requirement even for neutron within a limited core volume. At the same time, B_4C will produce γ rays with energy in about 480 keV after absorbing neutrons [51]. A heavier γ rays

Table 3: Radiation shielding performance at different layouts of shielding material.

	Without shielding	W-$Mg(BH_4)_2$ shielding	$Mg(BH_4)_2$ -W shielding
Neutron flux (n/(cm^2·s))	1.13438*E* + 11	2.53589*E* + 02	3.41285*E* + 02
Neutron radiation dose (rem/h)	1.35225*E* + 06	3.43283*E* − 02	4.08886*E* − 02
Photon flux (p/(cm^2·s))	3.19944*E* + 10	1.53725*E* + 04	2.34865*E* + 04
Photon radiation dose (rem/h)	4.16667*E* + 04	4.10371*E* − 02	4.7371*E* − 02

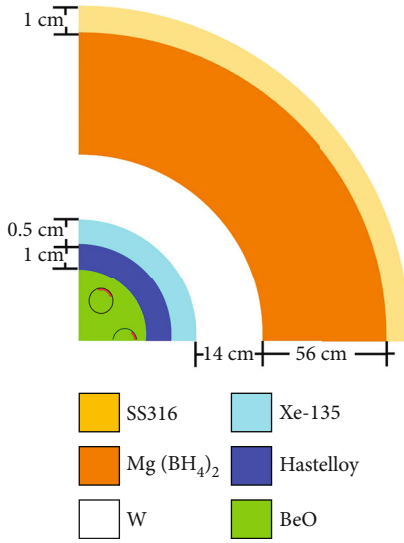

Figure 16: Layout of radiation shielding material for HX-micro-MSR.

shielding materials must be hence placed outside the B_4C material to shield the γ rays, leading to a significant increase in the weight of core. With the above considerations, an advanced neutron shield material, i.e., $Mg(BH_4)_2$, is adopted and evaluated [52]. The density of $Mg(BH_4)_2$ is only 1.48 g/cm^3, and the atomic fraction of hydrogen, boron, magnesium in $Mg(BH_4)_2$ is 72.73%, 18.18%, and 9.09%, respectively, and the enrichment of ^{10}B in B is 90%. The dose changing with the thickness of $Mg(BH_4)_2$ is shown in Figure 15.

It can be seen that $Mg(BH_4)_2$ presents a much higher neutron shielding ability compared with that of W, Pb, and B_4C but is inferior to W and Pb in terms of photon shielding. $Mg(BH_4)_2$ together with W is hence taken to effectively shield both the neutrons and photons to meet the shielding criterion. As demonstrated in Figures 14 and 15, a layer of W with thickness in 16 cm and a layer of $Mg(BH_4)_2$ with thickness in 60 cm can reduce the photon radiation intensity and neutron radiation intensity to 0.18 rem/h and 0.11 rem/h, respectively. Simply stacking them might satisfy the criteria of radiation, while the thickness of 76 cm will result to the core size exceeding the limitation of space, since the outer radius of reflector already achieves 47.3 cm. Finally, relatively small change of W thickness (14 cm) while reducing the $Mg(BH_4)_2$ thickness to 56 cm is performed to ensure dimensional compliance. Two layouts with the W placed in front of or behind $Mg(BH_4)_2$, respectively, indicated as W-$Mg(BH_4)_2$ and $Mg(BH_4)_2$-W shielding, are investigated as demonstrated in Table 3. The layout of W-$Mg(BH_4)_2$ shielding presents a better performance in both neutrons and photons shielding since heavy nuclei reduce neutron energy, which subsequently reduces the burden of $Mg(BH_4)_2$ and the generation of secondary photons in $Mg(BH_4)_2$. On the other hand, because of the large density of W (18.5 g/cm^3), the weight of reactor will reach to 133 tonnes as W is placed behind $Mg(BH_4)_2$ which is far beyond the weight limitation of 38 tonnes. The layout of W-$Mg(BH_4)_2$ is hence selected for the design of HX-micro-MSR as shown in Figure 16. In this case, the core has a weight of 35 tonnes, diameter of 242 cm, and length of 244 cm, which meet the requirements of the core design as introduced in Section 1.

Table 4: Optimized parameters of HX-micro MSR.

Parameters	Value of number
Reactor core	
Reactor diameter/length (cm)	242 × 244
Reactor mass (tonne)	35.00
Enrichment of U-235 (%)	61
Reflector thickness (cm)	23.00
SiC pipes	
Inner radius (cm)	0.40
Thickness (mm)	0.50
Length (cm)	49.00
Safety factor	6.10
Flow velocity (m/s)	7.10
Number of pipes	1050
Control drums	
Outer diameter (cm)	10.50
Thickness of B_4C (cm)	1.00
Shielding layer	
Thickness of Xe-135 layer (cm)	0.50
Thickness of W layer (cm)	14.00
Thickness of $Mg(BH_4)_2$ (cm)	56.00
Thickness of SS316 (cm)	1.00
Reactor performances	
Long burnup (years)	5
Deep shutdown margin ($)	15.74
Temperature coefficient (pcm/K)	-5.72
Radiation shielding (rem/h)	7.53*E* − 2

4.5. HX-Micro-MSR Specification. The main parameters of the optimized core is summarized in Table 4. It can be seen that all the design criteria are satisfied by the small

core size (241 cm in length × 262 cm in diameter), light weight (35 tonnes), long burnup (5 years), deep shutdown margin (\$7.5, $k_{\text{eff}} = 0.94997$), negative temperature coefficient (-5.72 pcm/K), and radiation shielding ($7.53E-2$ rem/h).

5. Conclusion

Micronuclear reactors (MNRs) have been attracting growing attention worldwide because of their flexibility in deployment. In this study, a novel micronuclear reactor employing He-Xe gas as the coolant while using fissile and fertile elements dissolved in molten salt as the fuel (referred to as HX-micro-MSR) is designed. Because of the usage of liquid fuel, HX-micro-MSR has a more simplified core structure compared with solid-fueled MNRs. The heated He-Xe gas from the core will be directly guided to the thermoelectric conversion system, forming a closed Brayton cycle which can provide a thermal efficiency higher than 40%. To significantly reduce the number of turbomachine stages while maintaining excellent thermal properties as helium, He-Xe gas having a molar mass of 40 g/mol with He in 72 mol% and Xe in 28 mol% is adopted. The neutron poison of Xe-135 produced in the core is online extracted and filled in the place surrounding the reflector to act as the neutron shielding layer. Based on this newly proposed MNR, the main components of the core, including the coolant pipe, reflector, control drum, and radiation shielding layer, are extensively analyzed and optimized to ensure that the designed core satisfies the criteria. The main conclusions extracted from the study are summarized in the following:

(1) The size of reactor system is 242 cm × 244 cm ($D \times H$), which is smaller than the standard containers and can be transported by trucks

(2) The total weight of the optimized system is 35 tonnes, complying with the constraints of land transportation

(3) The FOS of coolant pipe achieves 6.1, which can conservatively ensure the safety of coolant pipe even at a high operating pressure

(4) Negative fuel temperature coefficient of this system is -5.72 pcm/k, which can ensure the safety of the reactor system

(5) The k_{eff} of reactor can be kept under 0.95 as fully close to the six control drums, which can guarantee the core safety under accidents

(6) The shielding layer is composed of five materials, Hastelloy, Xe-135, W, $Mg(BH_4)_2$, and SS316, which can decrease the radioactivity surrounding the reactor to $7.53E-2$ rem/h to satisfy the radiation shielding criterion

Since thermal hydraulics plays an important role in the core performance, it will be coupled with neutronic calculation to further optimize the core design in the future. Meanwhile, accidents including leakage of fuel salt and reactor falling into the sea or lake, which would introduce a great core reactivity, will be extensively studied to ensure the safety of HX-micro-MSR.

Data Availability

The simulation data used to support the findings of this study were supplied by Hongkai Zhao under license and so cannot be made freely available. Requests for access to these data should be made to Hongkai Zhao (zhaohongkai@sinap.ac.cn).

Conflicts of Interest

The authors declare that they have no conflicts of interest.

Acknowledgments

This work is supported by the National Natural Science Foundation of China (Grant Nos. 11905285 and 12175300); Shanghai Natural Science Foundation (no. 20ZR1468700); Young Potential Program of Shanghai Institute of Applied Physics, Chinese Academy of Sciences (Grant No. SINAP-YXJH-202204); and Chinese TMSR Strategic Pioneer Science and Technology Project (Grant No. XDA02010000).

References

[1] J. E. Kelly, "Generation IV International Forum: A Decade of Progress through International Cooperation," *Progress in Nuclear Energy*, vol. 77, pp. 240–246, 2014.

[2] C. Forsberg and P. F. Peterson, "Basis for fluoride salt-cooled high-temperature reactors with nuclear air-Brayton combined cycles and firebrick resistance-heated energy storage," *Nuclear Technology*, vol. 196, no. 1, pp. 13–33, 2016.

[3] M. Margulis and E. Shwageraus, "Advanced gas-cooled reactors technology for enabling molten-salt reactors design - estimation of coolant impact on neutronic performance," *Progress in Nuclear Energy*, vol. 125, article 103382, 2020.

[4] M. Margulis and E. Shwageraus, "Advanced gas-cooled reactors technology for enabling molten-salt reactors design-optimisation of a new system," *Nuclear Engineering and Design*, vol. 385, article 111546, 2021.

[5] M. Margulis and E. Shwageraus, "Optimisation of AGR-like FHR fuel assembly using multi-objective particle swarm algorithm," *Journal of Nuclear Engineering*, vol. 2, no. 1, pp. 35–43, 2021.

[6] Z. Xing, P. Cosgrove, M. Margulis, and E. Shwageraus, "Design space exploration for salt-cooled reactor system: Part I-thermal hydraulic design," *Nuclear Engineering and Design*, vol. 393, article 111779, 2022.

[7] J. Křepel, B. Hombourger, C. Fiorina et al., "Fuel cycle advantages and dynamics features of liquid fueled MSR," *Annals of Nuclear Energy*, vol. 64, pp. 380–397, 2014.

[8] R. Testoni, A. Bersano, and S. Segantin, "Review of nuclear microreactors: Status, potentialities and challenges," vol. 138, Article ID 103822, 2021.

[9] G. Sun, M. Cheng, and Z. Dai, "Preliminary analysis of fuel management for a small modular molten salt fast reactor," *Nuclear Techniques*, vol. 39, 2016.

[10] M.-L. Tan, G.-F. Zhu, Y. Zou, X.-H. Yu, and Y. Dai, "Research on the effect of the heavy nuclei amount on the temperature reactivity coefficient in a small modular molten salt reactor," *Nuclear Science and Techniques*, vol. 30, no. 9, 2019.

[11] W. B. Cottrell, *Reactor program of the aircraft nuclear propulsion. ORNL-1234*, ORNL, USA, 1952.

[12] A. M. Weinberg and C. B. Ellis, *The aircraft nuclear propulsion program and general reactor technology. ORNL-0528*, OPNL, USA, 1950.

[13] C. Wang, M. Liu, D. Zhang, S. Qiu, G. H. Su, and W. Tian, "Experimental study on transient performance of heat pipe-cooled passive residual heat removal system of a molten salt reactor," *Progress in Nuclear Energy*, vol. 118, article 103113, 2020.

[14] C. Wang, Y. Yang, M. Liu et al., "Transient thermal-hydraulic analysis of heat pipe cooled passive residual heat removal system of molten salt reactor," *International Journal of Energy Research*, vol. 45, no. 2, pp. 1599–1612, 2021.

[15] É. F. de Araújo, G. B. Ribeiro, and L. N. F. Guimarães, "Design optimization of a cross-flow He-Xe recuperator through second law analysis," *Thermal Science and Engineering Progress*, vol. 19, article 100568, 2020.

[16] O. Olumayegun, M. Wang, and G. Kelsall, "Closed-cycle gas turbine for power generation: a state-of-the-art review," *Fuel*, vol. 180, pp. 694–717, 2016.

[17] J. Kikstra, *Conceptual Design for the Energy Conversion System of the ACACIA Nuclear Cogeneration Plant*, Netherlands Energy Research Foundation ECN, 1998.

[18] W. Van Niekerk, P. Rousseau, and G. Greyvenstein, "Operation and Simulation of a Three-Shaft, Closed-Loop, Brayton Cycle Model of the PBMR Power Plant," in *Proceedings of the International Congress on Advances in Nuclear Power Plants (ICAPP'03)*, Cordoba, Spain, 2003.

[19] M. S. El-Genk and J.-M. Tournier, "Noble gas binary mixtures for gas-cooled reactor power plants," *Nuclear Engineering and Design*, vol. 238, no. 6, pp. 1353–1372, 2008.

[20] J. M. Tournier, M. El-Genk, and B. Gallo, "Best Estimates of Binary Gas Mixtures Properties for Closed Brayton Cycle Space Applications," in *4th International Energy Conversion Engineering Conference and Exhibit (IECEC)*, p. 4154, San Diego, CA, USA, 2006.

[21] L. S. Mason and J. G. Schreiber, "A historical review of Brayton and Stirling power conversion technologies for space applications," in *Space Nuclear Conference 2007*no. E-1614, pp. 367–373, Boston, MA, 2007.

[22] J.-C. Worms, E. Cliquet-Moreno, E. Detsis et al., *MEGAHIT: Megawatt Highly EFficient Technologies for Space Power and Propulsion Systems for Long-Duration Exploration Missions-Advanced Propulsion Roadmap for Horizon 2020*, Transactions of the American Nuclear Society, 2013.

[23] W. Kesternich, "A possible solution of the problem of helium embrittlement," *Journal of Nuclear Materials*, vol. 127, no. 2-3, pp. 153–160, 1985.

[24] Ministry of Transport of the People's Republic of China, *Decision of the Ministry of Transport on amending the Regulations on the Administration of Over-Limit Transport Vehicles Driving on Highways*, Ministry of Transport of the People's Republic of China, 2021.

[25] B. Hong, *Core Physics Study of Lithium Heat-Pipe Cooled Space Reactor in Chinese*, University of Chinese Academy of Sciences, 2018.

[26] P. Bajpai, S. Lorenzi, and A. J. T. E. P. J. P. Cammi, "A multi-physics model for analysis of inert gas bubbles in molten salt fast reactor," vol. 135, pp. 1–22, 2020.

[27] C. Yu, J. Wu, C. Zou, X. Cai, Y. Ma, and J. Chen, "Thorium utilization in a small modular molten salt reactor with progressive fuel cycle modes," *International Journal of Energy Research*, vol. 43, no. 8, pp. 3628–3639, 2019.

[28] C. Xu, F. Kong, D. Yu, J. Yu, and M. S. J. E. Khan, "Influence of non-ideal gas characteristics on working fluid properties and thermal cycle of space nuclear power generation system," *Energy*, vol. 222, article 119881, 2021.

[29] G.-C. Li, Y. Zou, C.-G. Yu, J.-L. Han, J.-G. Chen, and H.-J. Xu, "Influences of 7Li enrichment on Th–U fuel breeding for an Improved Molten Salt Fast Reactor (IMSFR)," *Nuclear Science and Techniques*, vol. 28, 2017.

[30] W.-W. Xu, F. Xia, L. Chen, M. Wu, T. Gang, and Y. Huang, "High-temperature mechanical and thermodynamic properties of silicon carbide polytypes," *Journal of Alloys and Compounds*, vol. 768, pp. 722–732, 2018.

[31] Y. Katoh, D. F. Wilson, and C. Forsberg, *Assessment of Silicon Carbide Composites for Advanced Salt-Cooled Reactors*, Oak Ridge National Laboratory, 2007.

[32] H. Ogihara, H. Wang, and T. Saji, "Electrodeposition of Ni-B/SiC composite films with high hardness and wear resistance," *Applied Surface Science*, vol. 296, pp. 108–113, 2014.

[33] M. El-Genk and J.-M. Tournier, "Selection of Noble Gas Binary Mixtures for Brayton Space Nuclear Power Systems," in *4th International Energy Conversion Engineering Conference and Exhibit (IECEC)*, p. 4168, San Diego, CA, USA, 2006.

[34] M. S. Freedman, A. Turkevich, R. M. Adams, N. Sugarman, S. Raynor, and L. G. Stang, "The slow-neutron absorption cross-section of 9·2-H Xe135 by the method of negative activation," *Journal of Inorganic and Nuclear Chemistry*, vol. 2, pp. 271–285, 1956.

[35] H.-H. Lee, *Finite Element Simulations with ANSYS Workbench 18*, SDC publications, 2018.

[36] W. A. Wieselquist, R. A. Lefebvre, and M. A. Jessee, *SCALE code system*, Oak Ridge National Lab.(ORNL), Oak Ridge, TN, USA, 2020.

[37] S. Xia, J. Chen, W. Guo et al., "Development of a molten salt reactor specific depletion code MODEC," *Annals of Nuclear Energy*, vol. 124, pp. 88–97, 2019.

[38] L.-Y. He, Y. Cui, L. Chen et al., "Effect of reprocessing on neutrons of a molten chloride salt fast reactor," *Nuclear Science and Techniques*, vol. 34, no. 3, 2023.

[39] J. Wu, J. Chen, X. Cai et al., "A review of molten salt reactor multi-physics coupling models and development prospects," *Energies*, vol. 15, no. 21, p. 8296, 2022.

[40] J. Wu, C. Zou, C. Yu, X. Cai, and J. Chen, "Study of natural uranium utilization in a heavy water moderated molten salt reactor," *Progress in Nuclear Energy*, vol. 146, article 104144, 2022.

[41] P. A. Cundall and O. D. J. G. Strack, "A discrete numerical model for granular assemblies," *Geotechnique*, vol. 29, no. 1, pp. 47–65, 1979.

[42] Y. Tan, D. Yang, and Y. Sheng, "Discrete element method (DEM) modeling of fracture and damage in the machining process of polycrystalline SiC," *Journal of the European Ceramic Society*, vol. 29, no. 6, pp. 1029–1037, 2009.

[43] The Engineering ToolBox, *Factors of Safety - FOS*, 2010, https://www.engineeringtoolbox.com/factors-safety-fos-d_1624.html.

[44] J. Wu, J. Chen, X. Kang et al., "A novel concept for a molten salt reactor moderated by heavy water," *Annals of Nuclear Energy*, vol. 132, pp. 391–403, 2019.

[45] C. Y. Zou, X. Z. Cai, D. Z. Jiang et al., "Optimization of temperature coefficient and breeding ratio for a graphite-moderated molten salt reactor," *Nuclear Engineering and Design*, vol. 281, pp. 114–120, 2015.

[46] J. C. King and M. S. El-Genk, "Submersion-subcritical safe space (S4) reactor," *Nuclear Engineering and Design*, vol. 236, no. 17, pp. 1759–1777, 2006.

[47] S. Azimkhani, F. Zolfagharpour, and F. Ziaie, "Investigation of reflection properties of applied reflectors for thermal neutrons by considering the albedo and spectral shift," *Progress in Nuclear Energy*, vol. 100, pp. 192–196, 2017.

[48] J. Li, Q. Zhou, Y. Xia et al., "Study on reactivity control strategies for the thermoelectric integrated space nuclear reactor," *Annals of Nuclear Energy*, vol. 145, article 107607, 2020.

[49] C. Forsberg, L. Hu, P. Peterson, and K. Sridharan, *Fluoride-Salt-Cooled High-Temperature Reactor (FHR) for Power and Process Heat*, Massachusetts Inst. of Technology (MIT), 2015.

[50] H. Li, *Fundamentals of Radiation Protection*, Atomic Energy Press, Beijing, China, 1982.

[51] C.-D. Wen, "Physics for Radiation Protection—A Handbook 2nd Edition," *Medical Physics*, vol. 33, no. 12, 2006.

[52] N. Hatefi Moadab and M. Kheradmand Saadi, "Optimization of an Am-Be neutron source shield design by advanced materials using MCNP code," *Radiation Physics and Chemistry*, vol. 158, pp. 109–114, 2019.